

Toroidal charge exchange recombination spectroscopy measurements on MST^{a)}

R. M. Magee,^{1,b)} D. J. Den Hartog,¹ G. Fiksel,^{1,c)} S. T. A. Kumar,¹ and D. Craig²

¹University of Wisconsin, 1150 University Avenue, Madison, Wisconsin 53706, USA

²Wheaton College, 501 College Avenue, Wheaton, Illinois 60187, USA

(Presented 18 May 2010; received 15 May 2010; accepted 21 June 2010;

published online 11 October 2010)

Charge exchange recombination spectroscopy measurements of the poloidal component of the C^{+6} temperature and flow in the Madison Symmetric Torus have been vital in advancing the understanding of the ion dynamics in the reversed field pinch. Recent work has expanded the diagnostic capability to include toroidal measurements. A new toroidal view overcomes a small signal-to-background ratio (5%–15%) to make the first localized measurements of the parallel component of the impurity ion temperature in the core of the reversed field pinch. The measurement is made possible through maximal light collection in the optical design and extensive atomic modeling in the fitting routine. An absolute calibration of the system allowed the effect of Poisson noise in the signal on line fitting to be quantified. The measurement is made by stimulating emission with a recently upgraded 50 keV hydrogen diagnostic neutral beam. Radial localization is ~ 4 cm², and good temporal resolution (100 μ s) is achieved by making simultaneous emission and background measurements with a high-throughput double-grating spectrometer. © 2010 American Institute of Physics. [doi:10.1063/1.3478665]

I. INTRODUCTION

The ability to make fast (10 μ s), localized (~ 1 cm²) charge exchange recombination spectroscopy (CHERS) measurements of the poloidal component of the impurity ion temperature and flow in the Madison Symmetric Torus (MST) (Ref. 1) has been used to address the long observed anomalous ion heating problem. Although ion heating had been observed in the reversed field pinch (RFP) for decades,² it was CHERS profile measurements that first definitively showed magnetic reconnection to be the causal agent.³ The addition of a complementary toroidal view promises to further advance this line of research. In particular, it will allow a detailed comparison of the parallel and perpendicular ion temperature in the core of MST to provide new insight into the as-yet-unknown magnetic reconnection heating mechanism.

CHERS measurements on MST are particularly challenging because the charge exchange signal is small relative to the large and fast changing background in which it is embedded. In typical tokamak systems, the emission is stimulated with a high power neutral beam, providing signal levels which are much larger than the background.⁴ In MST, the emission is stimulated with a low power diagnostic neutral beam. This allows Ohmically heated RFP discharges to be studied, but necessitates that a background measurement also be made. Background subtraction via beam modulation,

used elsewhere,⁵ is unfeasible here because the frequencies at which the interesting physics occurs (≥ 10 kHz) are much faster than typical modulation frequencies.

The geometry of the CHERS system on MST is illustrated in Fig. 1. The measurement locations (i.e., the intersection of the neutral beam and the line-of-sight) are the same for each view (11 locations spaced ~ 10 cm apart from $-0.9 < r/a < 0.8$), although low signal levels prevent some chords from being used. Figure 1 also illustrates the principal design challenge of the toroidal view: the longer line-of-sight through the plasma results in a lower signal-to-background ratio. The success of the measurement depended on the optimization of each component of the system. We begin with a review of the spectrometer design (Sec. II) and line-fitting algorithm (Sec. III), which have been described elsewhere.^{6,7} The optical design of the toroidal view is described in Sec. IV. The diagnostic neutral beam was upgraded, some details of which are presented in Sec. V. Finally, the CHERS system was recently absolutely calibrated, which allowed the signal-to-noise level to be quantified, and the response of the fitting code to noisy data explored (Sec. VI). We find that the measurement is robust to the Poisson noise at relative signal levels of $\geq 1\%$.

II. SPECTROMETER

The principal spectrometer design requirements were that it should be able to make two simultaneous measurements, have high throughput and good wavelength resolution, and have a fast data collection rate. The resulting double-grating, Czerny–Turner duo spectrometer achieves an étendue of 0.80 mm² sr and a good wavelength resolution ($\lambda/\Delta\lambda=5600$) through the use of two large area (220 \times 220 mm²) gratings (3600 grooves/mm). The acceptance

^{a)} Contributed paper, published as part of the Proceedings of the 18th Topical Conference on High-Temperature Plasma Diagnostics, Wildwood, New Jersey, May 2010.

^{b)} Electronic mail: rmmagee@wisc.edu.

^{c)} Present address: Laboratory for Laser Energetics, University of Rochester.

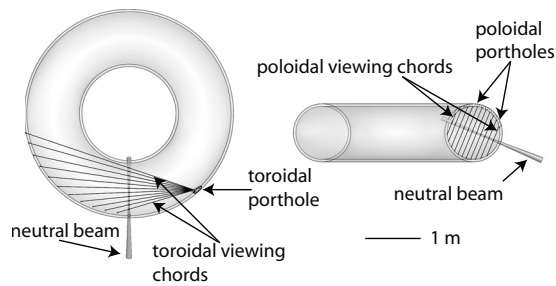


FIG. 1. A top down view of the toroidal viewing chords (left) and a poloidal cross-section of the poloidal viewing chords (right) illustrate the longer path length (and larger line-integrated background signal) in the toroidal view relative to the poloidal. The toroidal chord, seventh from the bottom, intersects the neutral beam at the magnetic axis, which is the location of the T_{par} measurement shown in Fig. 3.

cone of the spectrometer is $f/4.5$. The high data rate (100 kHz) is made possible by the use of photo-multiplier tubes (PMTs) rather than charged-coupled devices at the image plane. Each view is composed of 16 spectral channels covering ~ 0.5 nm at 343.3 nm. The channel width, 0.043 nm, is small compared to the Doppler broadening observed in typical MST discharges.⁷

The spectrometer is calibrated in relative wavelength and relative amplitude annually with a Cd lamp. The Cd I doublet at 346.62 and 346.77 nm is scanned across the exit plane by scanning the diffraction gratings at constant velocity. The time delay between the appearance of the doublet in one channel and its appearance in the neighboring channel is converted to wavelength using the known doublet wavelength spacing. The variation in line amplitude from channel to channel is used to determine the relative sensitivity of each channel. The entire system has recently been absolutely calibrated, which is described in Sec. VI.

III. FITTING METHOD

The line-fitting algorithm proceeds by first creating a model of the emission. The background is assumed to be a mixture of electron impact (EI) excited O VI (343.4 nm) and C VI (343.3 nm) emission, both corresponding to the $n=7$ to $n=6$ transition. There is substantial fine-structure broadening of the line due to L-S coupling. The relative intensities of the various components are determined by the temperature and density of the plasma and calculated with the atomic data and analysis structure (ADAS) database.⁸ The Doppler width and shift and overall amplitude are the fitting parameters. These are adjusted through a chi-square minimization routine until the best fit is found (Fig. 2). The errors in the data are assumed to be due to Poisson noise.

The next step is to model the total emission with an EI component identical to the background plus a charge exchange (CX) component. Unlike the EI component, the CX component is assumed to be purely C VI. This is due to disparities in the EI and CX cross-sections. The EI excitation cross-section is much larger for oxygen than for carbon ($\sigma_{\text{O,EI}} \sim 10\text{--}20\sigma_{\text{C,EI}}$), while the CX cross-sections for the two species are comparable.⁸ This means that the much lower concentration of oxygen empirically found in MST plasmas contribute to the EI emission but not the CX.

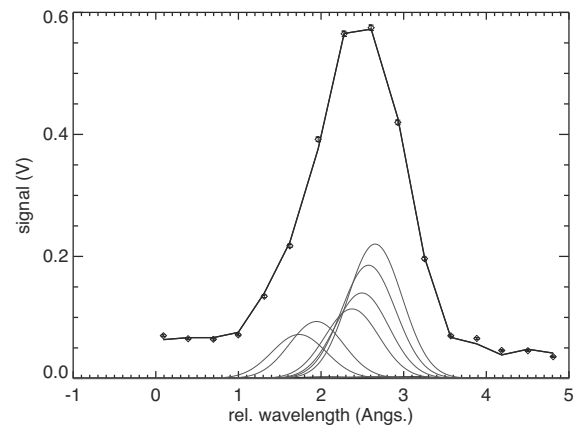


FIG. 2. The relative intensities of the fine structure components (gray) of the electron impact excitation of the O VI line are modeled by ADAS. These components are Doppler broadened and shifted by an equal amount until their sum (black) best fits the experimental data (diamonds). The error bars on the data points represent the Poisson noise.

The line-integrated C^{+5} temperature, velocity, and density are calculated from the fitting parameters of the background emission, and the local C^{+6} temperature, velocity, and density from the CX emission.⁶

IV. TOROIDAL VIEW OPTICAL DESIGN

Because of porthole vignetting, the ray bundles for off-axis viewing locations are elliptical, and therefore cannot be described by a single $f/\#$. We desired that the $f/\#$ corresponding to the minor axis of the ellipse be $\lesssim 4.5$ for most viewing chords. A fused-silica 101.6 mm with $f=250$ mm most nearly satisfied this criterion.

The spatial resolution of the measurement (~ 4 cm²) is set by the magnification of the lens. This was confirmed experimentally during the alignment of the optical system. Reverse illumination of the optical train with a $f/4.5$ light source the same size as the fiber face produced a focused image on a target probe with $r \sim 4$ cm².

The line-of-sight from the central toroidal viewing chord and the magnetic axis intersect at a small angle (8°), which means that Doppler shifts from this measurement location are dominated by the motion of the plasma parallel to the equilibrium magnetic field (perpendicular motion contributes only 2%). This effective parallel C VI ion temperature is shown in Fig. 3, averaged over many discharges, during the course of a magnetic reconnection heating event. The heating is comparable to the measured perpendicular heating in low density plasmas.

V. DIAGNOSTIC NEUTRAL BEAM UPGRADE

The small signal-to-background ratio expected from the toroidal view motivated an upgrade to the diagnostic neutral beam.⁹ An attempt was made to decrease the angular divergence and increase the beam current, both of which should increase the charge exchange signal, $S \sim I_b/r_b$ (I_b is the beam current and r_b is the radius of the beam at the measurement location). The beam current, I_b , was increased by nearly a factor of 2 from ~ 2.5 to ~ 5 A. The geometric divergence of the beam was decreased from 46 to 32 mrad. The total divergence of the beam, however, also includes the random

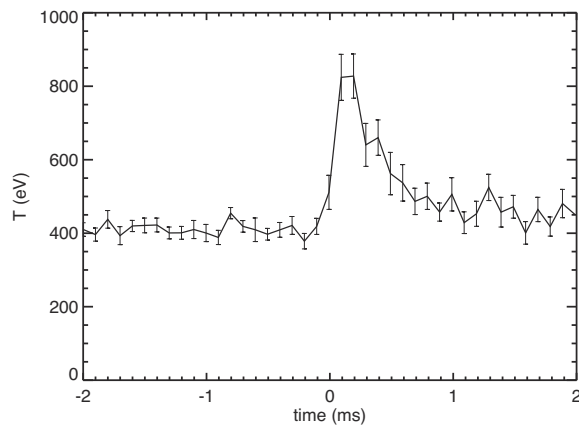


FIG. 3. The local C VI temperature measured on the magnetic axis ($r/a = 0$) of MST during a magnetic reconnection heating event. The temperature is obtained by averaging together 56 similar discharges and the error bars are the standard deviation of the mean.

divergence due to the finite temperature of the source plasma and the scattering of source ions before extraction. An unforeseen consequence of the beam upgrade was an increase in this quantity from 15 to 18 mrad. This resulted in the beam radius, r_b at the measurement location also increasing by nearly a factor of 2, so no charge exchange signal increase has been observed. Work continues to further increase the beam current to overcome the larger radius.

VI. THE EFFECT OF POISSON NOISE

An absolute calibration of the system has been performed by illuminating the entrance fibers of the spectrometer through a UG-1 optical filter and fused-silica lens setup as in the experiment with an integrating sphere. It was found that the amplified PMT signal is related to the incident light by $1 \text{ V} = 8.9 \times 10^{10} \text{ photons}/\text{\AA}/\text{s}$ near 343 nm. We use this information to create synthetic data to investigate the effect of small signal level on the accuracy of the fitting routine. As described above, the fitting routine fits a model of the total emission (CX+EI) to the data, so one may expect that as long as the number of charge exchange photons (N_{cx}) is larger than the noise on the total emission ($\sqrt{N_{\text{tot}}}$), the signal can be extracted.

The simulated data are created by convolving the ideal line, made up of an EI excited background and CX component (with $N_{\text{tot}} = 10^4$), with the transfer functions of the spectrometer channels and adding the Poisson noise. These data are fed back to the code with varying levels of charge exchange signal. The results are shown in Fig. 4. T_{meas}/T is the ratio of the fit temperature to the input temperature. We find that for signal levels $R \geq 1.3\%$, the fitting routine is able to extract the correct average temperature ($T_{\text{meas}}/T = 1.0$). This is slightly higher than the Poisson noise on the central channel. The larger relative Poisson noise on the off-peak channels increases the signal level required for accurate fitting. At higher temperatures of 1200 eV (black curve) the standard deviation (calculated as the square root of the variance in ~ 200 realizations of the line fitting) is large for this signal level. We also note that for $R \leq 1.3\%$ the fitting code tends to underestimate high temperatures ($T_{\text{meas}}/T < 1$) and overestimate low temperatures ($T_{\text{meas}}/T > 1$).

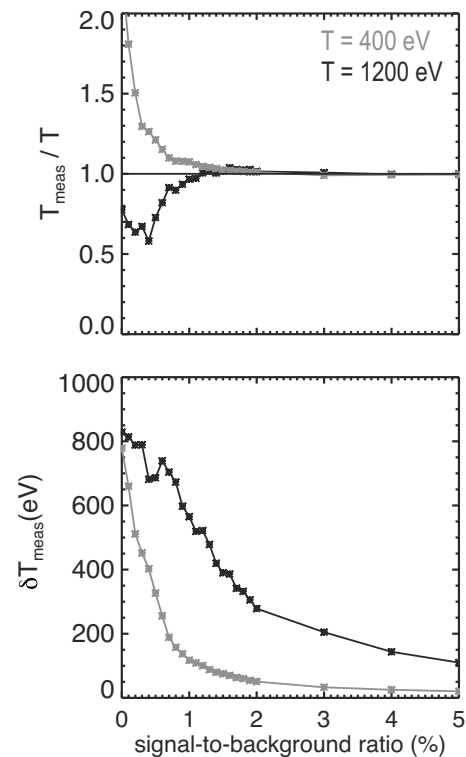


FIG. 4. The ratio of the fit temperature to the input temperature plotted against relative signal level R (top) shows that the number of photons collected is high enough that an accurate average temperature can be obtained with only $R \sim 1.3\%$. The standard deviation in that average (bottom) is large at low R .

In the experiment, the signal-to-background level is 5%–15% for the toroidal view and 15%–25% for the poloidal. The above results demonstrate that the fitting algorithm is robust to Poisson noise for these signal levels.

ACKNOWLEDGMENTS

The authors would like to thank Sanjay Gangadhara and David Ennis for their work in developing the CHERS system on MST and Pyotr Deichuli at the Budker Institute for Nuclear Physics for his help in troubleshooting and maintaining the neutral beam. This work was supported by the U.S. Department of Energy and the National Science Foundation.

- ¹R. N. Dexter, D. W. Kerst, T. W. Lovell, S. C. Prager, and J. C. Sprott, *Fusion Technol.* **19**, 131 (1991).
- ²B. B. Jones and R. Wilson, *Nucl. Fusion Suppl.* **3**, 889 (1962).
- ³S. Gangadhara, D. Craig, D. A. Ennis, D. J. Den Hartog, G. Fiksel, and S. C. Prager, *Phys. Plasmas* **15**, 056121 (2008).
- ⁴R. C. Isler, *Plasma Phys. Controlled Fusion* **36**, 171 (1994).
- ⁵M. Reich, E. Wolfrum, J. Schweinzer, H. Ehmler, L.D. Horton, J. Neuhauser, and ASDEX Upgrade Team, *Plasma Phys. Controlled Fusion* **46**, 797 (2004).
- ⁶S. Gangadhara, D. Craig, D. A. Ennis, and D. J. Den Hartog, *Rev. Sci. Instrum.* **77**, 10F109 (2006).
- ⁷D. Craig, D. J. Den Hartog, D. A. Ennis, S. Gangadhara, and D. Holly, *Rev. Sci. Instrum.* **78**, 013103 (2007).
- ⁸H. P. Summers, *The ADAS User Manual, version 2.6*, www.adas.ac.uk.
- ⁹G. F. Abdrashitov, V. I. Davydenko, P. P. Deichuli, D. J. Den Hartog, G. Fiksel, A. A. Ivanov, S. A. Korepanov, S. V. Murakhtin, and G. I. Shulzhenko, *Rev. Sci. Instrum.* **72**, 594 (2001).